Comput. Mech. (2006) 38: 469–481
DOI 10.1007/s00466-005-0025-6

ORIGINAL PAPER

Tayfun E. Tezduyar · Masayoshi Senga · Darby Vicker

Computation of inviscid supersonic flows around cylinders and spheres with the SUPG formulation and $YZ\beta$ shock-capturing

Received: 09 October 2005/ Accepted: 29 October 2005 / Published online: 18 January 2006

Abstract Numerical experiments with inviscid supersonic flows around cylinders and spheres are carried out to evaluate the stabilization and shock-capturing parameters introduced recently for the Streamline–Upwind/Petrov–Galerkin (SUPG) formulation of compressible flows based on conservation variables. The tests with the cylinders are carried out for both structured and unstructured meshes. The new shock-capturing parameters, which we call "$YZ\beta$ Shock-Capturing", are compared to earlier SUPG parameters derived based on the entropy variables. In addition to being much simpler, the new shock-capturing parameters yield better shock quality in the test computations, with more substantial improvements seen for unstructured meshes with triangular and tetrahedral elements. Furthermore, the results obtained with $YZ\beta$ Shock-Capturing compare very favorably to those obtained with the well established OVERFLOW code.

Keywords Supersonic flows · Cylinders and spheres · SUPG stabilization · Stabilization parameter · Shock-capturing parameter

1 Introduction

The Streamline–Upwind/Petrov–Galerkin (SUPG) formulation of compressible flows is now used widely in computational fluid mechanics. Soon after the introduction of the SUPG formulation of incompressible flows [1, 2], the SUPG formulation of compressible flows was first introduced, in the context of conservation variables, in a NASA technical report [3]. A concise version of that was published as an AIAA paper [4], and a more thorough version with additional examples as a journal paper [5]. Following [3–5], the SUPG formulation for compressible flows was recast in entropy variables [6]. In doing that, the formulation was also supplemented with a shock-capturing (discontinuity-capturing) term. With numerous test problems, it was shown in [7, 8] that the SUPG formulation introduced in [3–5], when supplemented with a similar shock-capturing term, is very comparable in accuracy to the one that was recast in entropy variables. The stabilized formulation introduced in [9] for advection–diffusion–reaction equations also included a discontinuity-capturing term, and precluded augmentation of the SUPG effect by the discontinuity-capturing effect when the advection and discontinuity directions coincide.

The SUPG formulations involve a stabilization parameter that most researchers call "τ". This parameter includes a measure of the local length scale (also known as "element length"). Various τ definitions were proposed starting with those in [1, 2] and [3–5], followed by the one introduced in [9], and those proposed in the subsequently reported SUPG-based methods (see for example [10, 11]. In many cases, the "element length" was seen as an advection length scale. We call the SUPG formulation introduced in [3–5] for compressible flows "$(\text{SUPG})_{82}$", and the set of τ definitions introduced in conjunction with that "τ_{82}". In the computations reported in [7], $(\text{SUPG})_{82}$ was used with a slightly modified version of τ_{82}. The shock-capturing term used in those computations involved a shock-capturing parameter that we call "δ_{91}". Calculation of δ_{91} requires evaluation of the Jacobian matrix of the transformation from the entropy variables to the conservation variables. The computational cost associated with that is not trivial. Subsequent minor modifications of τ_{82} accounted for the interaction between the shock-capturing and the $(\text{SUPG})_{82}$ terms in a fashion similar to how it was done in [9] for advection–diffusion–reaction equations. All these slightly modified versions of τ_{82}, which we categorize as "$\tau_{82\text{-MOD}}$", have always been used with the same δ_{91}. A second element length scale, which is based on the solution gradient, was introduced in [12, 13]. This second element length was recognized as a diffusion length scale. Based on that, new

T. E. Tezduyar (✉) · M. Senga
Department of Mechanical Engineering, Rice University – MS 321
6100 Main Street, Houston, TX 77005, USA
E-mail: tezduyar@rice.edu; msenga@rice.edu

D. Vicker
Applied Aeroscience and CFD Branch NASA Johnson Space Center,
Houston, TX 77058, USA
E-mail: darby.vicker-1@nasa.gov

Table 1 Non-default parameters for the OVERFLOW computations

IDISS	4	Matrix dissipation
VEPSL	0.3	Matrix dissipation limit on linear eigenvalue
VEPSN	0.3	Matrix dissipation limit on nonlinear eigenvalue
SMOO	0.0	Spectral radius term

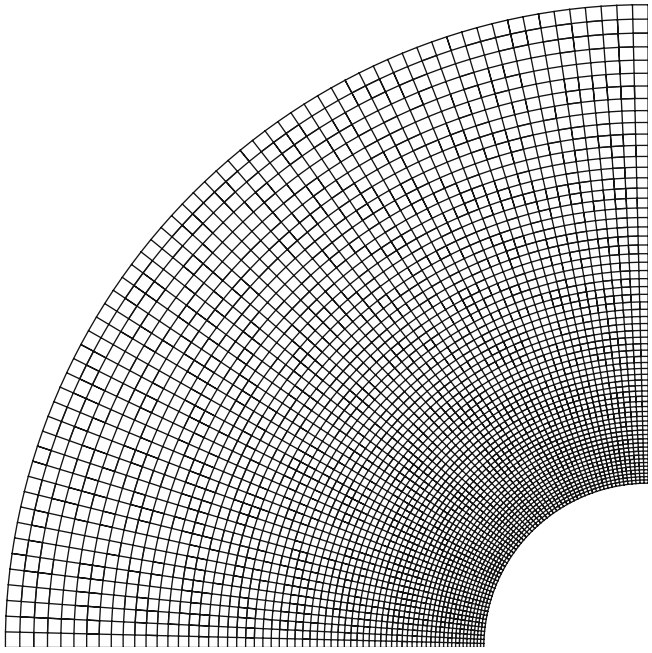

Fig. 1 Two-dimensional flow around a cylinder. Structured mesh with 4,096 quadrilateral elements and 4,225 nodes

stabilization parameters for the diffusive limit were introduced for incompressible flows in [13, 14].

New ways of calculating the SUPG τ values and shock-capturing parameters for compressible flows were introduced in [14, 15]. The new shock-capturing parameters, which we categorize as "$YZ\beta$ Shock-Capturing", are simpler and less costly to compute with than δ_{91}. They are based on scaled residuals and are defined with options for smoother or sharper shocks. A preliminary set of test computations with inviscid supersonic flows were reported in [16] for these new shock-capturing parameters. Those computations were limited to very simple 2D geometries and quadrilateral elements. A more comprehensive set of 2D test computations with inviscid supersonic flows were reported in [17]. Those tests with $YZ\beta$ Shock-Capturing involved different element types and mesh orientations. In this paper, we carry out numerical experiments with inviscid supersonic flows around cylinders and spheres to evaluate the performance of $YZ\beta$ Shock-Capturing in, what we find to be, more challenging test problems. Furthermore, we test a new version of $YZ\beta$ Shock-Capturing, which was originally introduced in [17] and which takes into account the Mach number and shock intensity across a shock. The 2D tests with the cylinders are carried out for both structured and unstructured meshes. In addition to comparing the $YZ\beta$ results to those obtained with τ_{82} and δ_{91}, for 2D

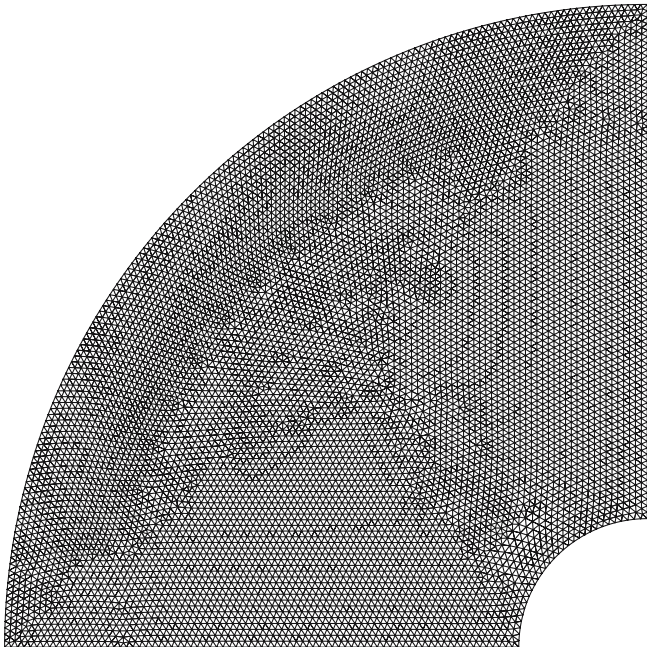

Fig. 2 Two-dimensional flow around a cylinder. Unstructured mesh with 17,520 triangular elements and 8,935 nodes

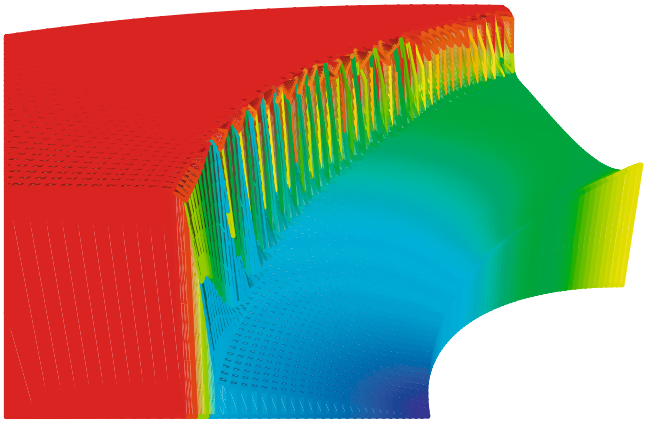

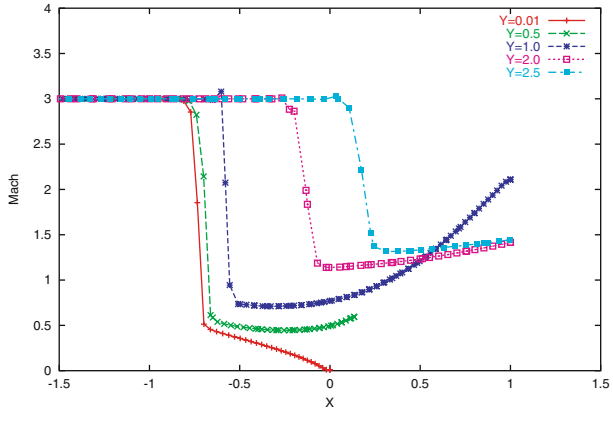

Fig. 3 Two-dimensional flow around a cylinder at $M = 3$. Mach elevation and line plots. Computed with the structured mesh and $YZ\beta$ Shock-Capturing with $b_{\mathrm{M}} = 2$, $b_{\mathrm{R}} = 0$

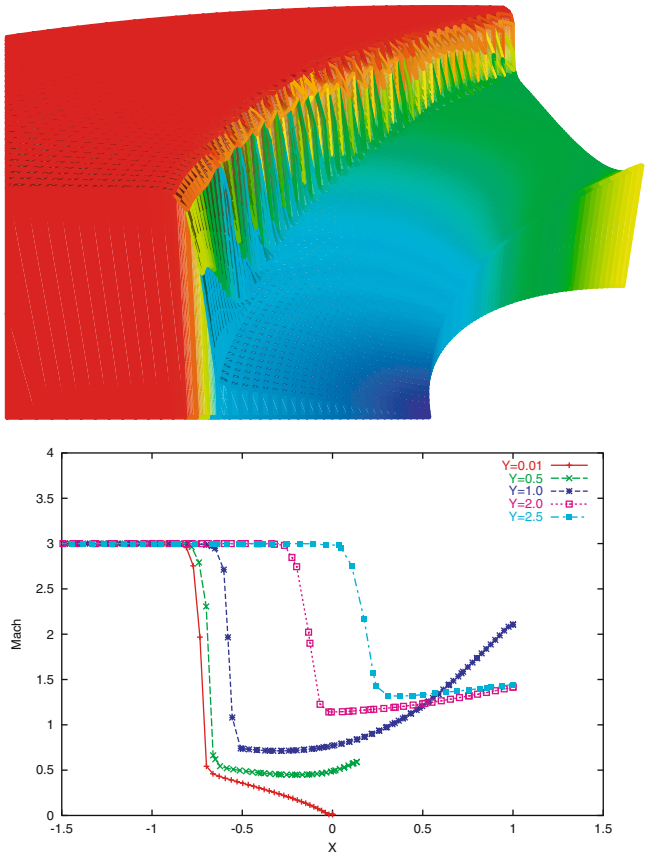

Fig. 4 Two-Dimensional flow around a cylinder at $M = 3$. Mach elevation and line plots. Computed with the structured mesh and $YZ\beta$ Shock-Capturing with $b_{\text{M}} = 1$, $b_{\text{R}} = 0$

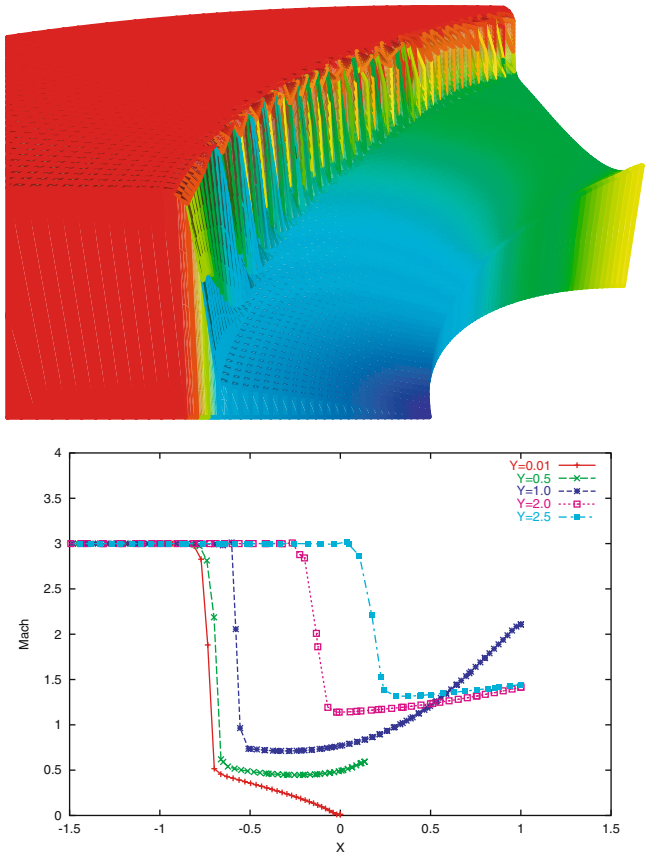

Fig. 5 Two-dimensional flow around a cylinder at $M = 3$. Mach elevation and line plots. Computed with the structured mesh and $YZ\beta$ Shock-Capturing with $b_{\text{M}} = 1$, $b_{\text{R}} = 1$, $\rho_{\text{sca}} = \rho_2$

structured meshes, we compare them to the results obtained with the OVERFLOW code [18].

2 Navier–Stokes equations of compressible flows

Let $\Omega \subset I\!R^{n_{\text{sd}}}$ be the spatial domain with boundary Γ, and $(0, T)$ be the time domain. The symbols ρ, $\mathbf{u}$, p and e will represent the density, velocity, pressure and the total energy, respectively.

The Navier–Stokes equations of compressible flows can be written on Ω and $\forall t \in (0, T)$ as

$$\frac{\partial \mathbf{U}}{\partial t} + \frac{\partial \mathbf{F}_i}{\partial x_i} - \frac{\partial \mathbf{E}_i}{\partial x_i} - \mathbf{R} = \mathbf{0}\,, \tag{1}$$

where $\mathbf{U} = (\rho, \rho u_1, \rho u_2, \rho u_3, \rho e)$ is the vector of conservation variables, and $\mathbf{F}_i$ and $\mathbf{E}_i$ are, respectively, the Euler and viscous flux vectors:

$$\mathbf{F}_i = \begin{pmatrix} u_i \rho \\ u_i \rho u_1 + \delta_{i1} p \\ u_i \rho u_2 + \delta_{i2} p \\ u_i \rho u_3 + \delta_{i3} p \\ u_i (\rho e + p) \end{pmatrix}, \quad \mathbf{E}_i = \begin{pmatrix} 0 \\ T_{i1} \\ T_{i2} \\ T_{i3} \\ -q_i + T_{ik} u_k \end{pmatrix}. \tag{2}$$

Here δ_{ij} are the components of the identity tensor $\mathbf{I}$, q_i are the components of the heat flux vector, and T_{ij} are the components of the Newtonian viscous stress tensor:

$$\mathbf{T} = \lambda(\nabla \cdot \mathbf{u})\mathbf{I} + 2\mu\boldsymbol{\varepsilon}(\mathbf{u}), \tag{3}$$

where λ and μ $(= \rho\nu)$ are the viscosity coefficients, ν is the kinematic viscosity, and $\boldsymbol{\varepsilon}(\mathbf{u})$ is the strain-rate tensor:

$$\boldsymbol{\varepsilon}(\mathbf{u}) = \frac{1}{2}\left((\nabla \mathbf{u}) + (\nabla \mathbf{u})^T\right). \tag{4}$$

It is assumed that $\lambda = -2\mu/3$. The equation of state used here corresponds to the ideal gas assumption. The term $\mathbf{R}$ represents all other components that might enter the equations, including the external forces.

Equation (1) can further be written in the following form:

$$\frac{\partial \mathbf{U}}{\partial t} + \mathbf{A}_i \frac{\partial \mathbf{U}}{\partial x_i} - \frac{\partial}{\partial x_i}\left(\mathbf{K}_{ij} \frac{\partial \mathbf{U}}{\partial x_j}\right) - \mathbf{R} = 0\,, \tag{5}$$

where

$$\mathbf{A}_i = \frac{\partial \mathbf{F}_i}{\partial \mathbf{U}}, \quad \mathbf{K}_{ij} \frac{\partial \mathbf{U}}{\partial x_j} = \mathbf{E}_i\,. \tag{6}$$

Appropriate sets of boundary and initial conditions are assumed to accompany Eq. (5).

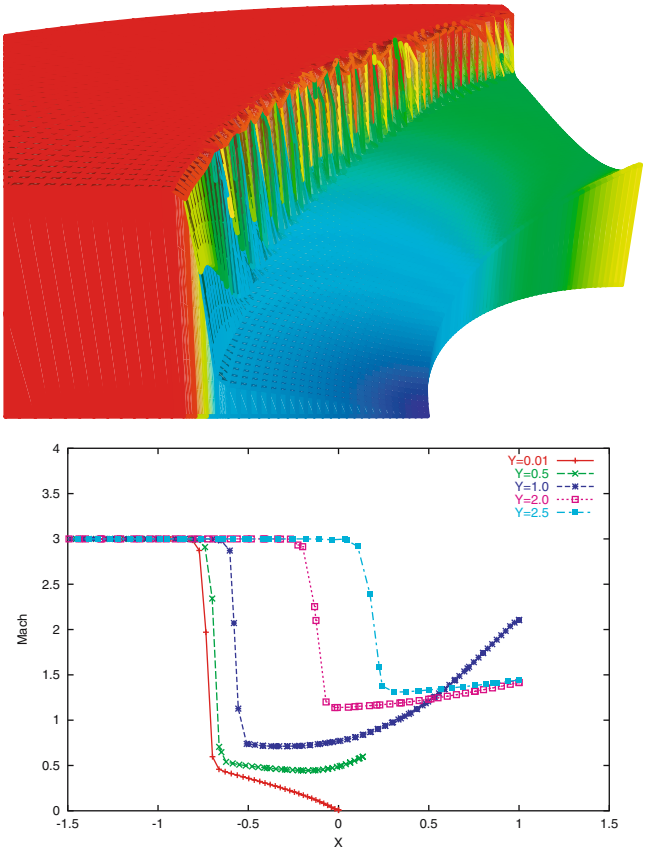

Fig. 6 Two-dimensional flow around a cylinder at $M = 3$. Mach elevation and line plots. Computed with the structured mesh and $\tau_{82\text{-MOD}}$ and δ_{91}

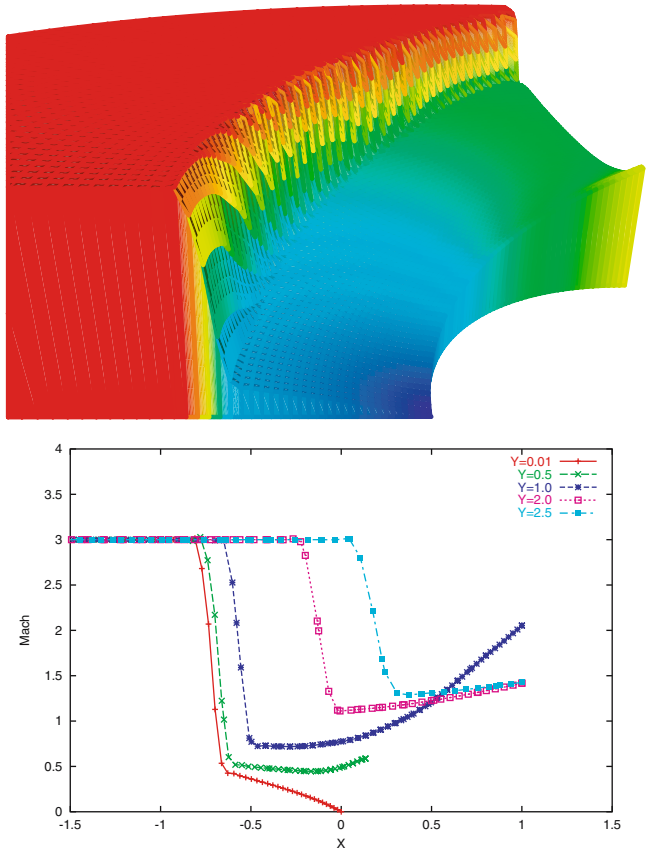

Fig. 7 Two-dimensional flow around a cylinder at $M = 3$. Mach elevation and line plots. Computed with the structured mesh and OVERFLOW

3 Semi-discrete and space–time SUPG formulations

In describing the semi-discrete SUPG formulation of Eq. (5), we assume that we have constructed some suitably-defined finite-dimensional trial solution and test function spaces $\mathcal{S}_{\mathrm{U}}^h$ and $\mathcal{V}_{\mathrm{U}}^h$. Based on that, the SUPG formulation [4, 5, 7] can be written as follows: find $\mathbf{U}^h \in \mathcal{S}_{\mathrm{U}}^h$ such that $\forall \mathbf{W}^h \in \mathcal{V}_{\mathrm{U}}^h$:

$$
\begin{aligned}
&\int_{\Omega} \mathbf{W}^h \cdot \left(\frac{\partial \mathbf{U}^h}{\partial t} + \mathbf{A}_i^h \frac{\partial \mathbf{U}^h}{\partial x_i} \right) \mathrm{d}\Omega \\
&\quad + \int_{\Omega} \left(\frac{\partial \mathbf{W}^h}{\partial x_i} \right) \cdot \left(\mathbf{K}_{ij}^h \frac{\partial \mathbf{U}^h}{\partial x_j} \right) \mathrm{d}\Omega \\
&\quad - \int_{\Gamma_{\mathrm{H}}} \mathbf{W}^h \cdot \mathbf{H}^h d\Gamma - \int_{\Omega} \mathbf{W}^h \cdot \mathbf{R}^h \mathrm{d}\Omega \\
&\quad + \sum_{e=1}^{n_{\mathrm{el}}} \int_{\Omega^e} \boldsymbol{\tau}_{\mathrm{SUPG}} \left(\frac{\partial \mathbf{W}^h}{\partial x_k} \right) \cdot \mathbf{A}_k^h \\
&\qquad \left[\frac{\partial \mathbf{U}^h}{\partial t} + \mathbf{A}_i^h \frac{\partial \mathbf{U}^h}{\partial x_i} - \frac{\partial}{\partial x_i} \left(\mathbf{K}_{ij}^h \frac{\partial \mathbf{U}^h}{\partial x_j} \right) - \mathbf{R}^h \right] \mathrm{d}\Omega \\
&\quad + \sum_{e=1}^{n_{\mathrm{el}}} \int_{\Omega^e} \nu_{\mathrm{SHOC}} \left(\frac{\partial \mathbf{W}^h}{\partial x_i} \right) \cdot \left(\frac{\partial \mathbf{U}^h}{\partial x_i} \right) \mathrm{d}\Omega = 0 \,. \qquad (7)
\end{aligned}
$$

Here $\mathbf{H}^h$ represents the natural boundary conditions associated with Eq. (5), and Γ_{H} is the part of the boundary where such boundary conditions are specified. The SUPG stabilization and shock-capturing parameters are denoted by $\boldsymbol{\tau}_{\mathrm{SUPG}}$ and ν_{SHOC}. They were discussed in Sect. 1 and will further be discussed in Sect. 4.

The space–time version of Eq. (7) can be written based on the Deforming-Spatial-Domain/Stabilized Space–Time (DSD/SST) formulation introduced in [19–21]. The finite element formulation of the governing equations is written over a sequence of N space–time slabs Q_n, where Q_n is the slice of the space–time domain between the time levels t_n and t_{n+1}. At each time step, the integrations involved in the finite element formulation are performed over Q_n. The finite element interpolation functions are discontinuous across the space–time slabs. We use the notation $(\cdot)_n^-$ and $(\cdot)_n^+$ to denote the values as t_n is approached from below and above respectively. Each Q_n is decomposed into space–time elements Q_n^e, where $e = 1, 2, \ldots, (n_{\mathrm{el}})_n$. The subscript n used with n_{el} is to account for the general case in which the number of space–time elements may change from one space–time slab to another. For each slab Q_n, we construct some suitably-defined finite-dimensional trial solution and test function spaces $(\mathcal{S}_{\mathrm{U}}^h)_n$ and $(\mathcal{V}_{\mathrm{U}}^h)_n$. In the computations reported here, we use first-order polynomials as interpolation functions. The subscript n implies that corresponding to different

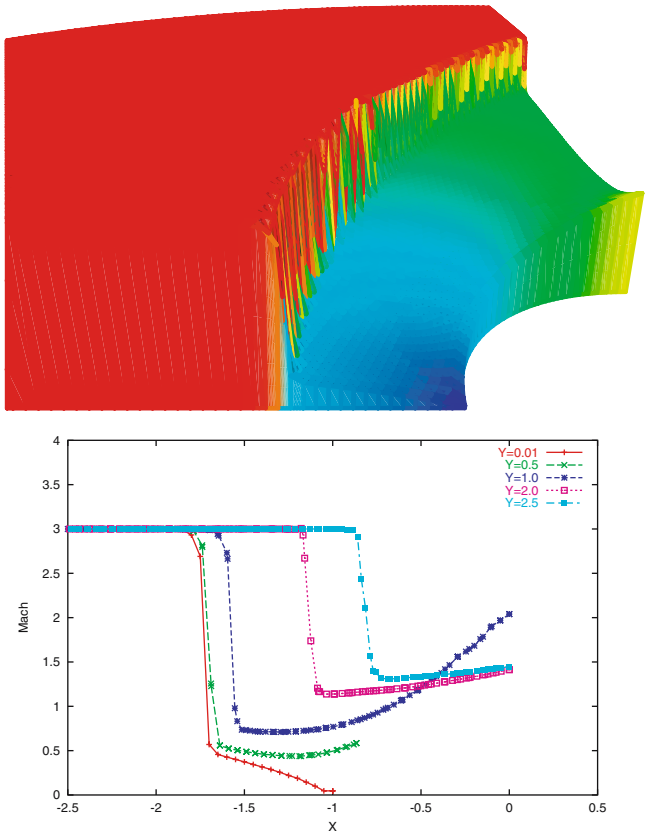

Fig. 8 Two-dimensional flow around a cylinder at $M = 3$. Mach elevation and line plots. Computed with the unstructured mesh and $YZ\beta$ Shock-Capturing with $b_{\mathrm{M}} = 2$, $b_{\mathrm{R}} = 0$

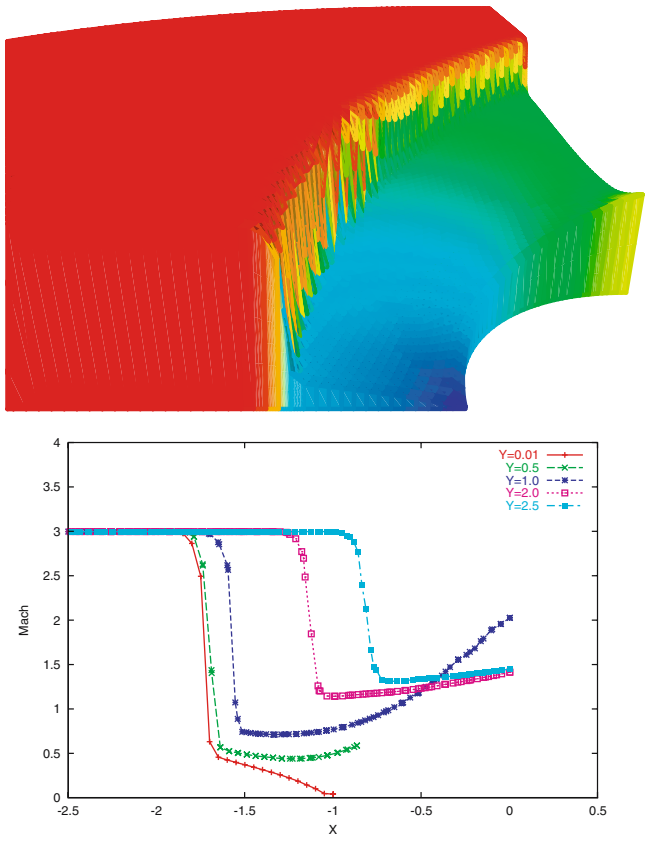

Fig. 9 Two-dimensional flow around a cylinder at $M = 3$. Mach elevation and line plots. Computed with the unstructured mesh and $YZ\beta$ Shock-Capturing with $b_{\mathrm{M}} = 1$, $b_{\mathrm{R}} = 0$

space–time slabs we might have different discretizations. The DSD/SST formulation of Eq. (5) can then be written as follows: given $(\mathbf{U}^h)_n^-$, find $\mathbf{U}^h \in (\mathcal{S}_{\mathrm{U}}^h)_n$ such that $\forall \mathbf{W}^h \in (\mathcal{V}_{\mathrm{U}}^h)_n$:

$$
\begin{aligned}
&\int_{Q_n} \mathbf{W}^h \cdot \left(\frac{\partial \mathbf{U}^h}{\partial t} + \mathbf{A}_i^h \frac{\partial \mathbf{U}^h}{\partial x_i} \right) \mathrm{d}Q \\
&+ \int_{Q_n} \left(\frac{\partial \mathbf{W}^h}{\partial x_i} \right) \cdot \left(\mathbf{K}_{ij}^h \frac{\partial \mathbf{U}^h}{\partial x_j} \right) \mathrm{d}Q \\
&- \int_{P_n} \mathbf{W}^h \cdot \mathbf{H}^h \mathrm{d}P - \int_{Q_n} \mathbf{W}^h \cdot \mathbf{R}^h \mathrm{d}Q \\
&+ \int_{\Omega} (\mathbf{W}^h)_n^+ \cdot \left((\mathbf{U}^h)_n^+ - (\mathbf{U}^h)_n^- \right) \mathrm{d}\Omega \\
&+ \sum_{e=1}^{(n_{\mathrm{el}})_n} \int_{Q_n^e} \boldsymbol{\tau}_{\mathrm{SUPG}} \left(\frac{\partial \mathbf{W}^h}{\partial x_k} \right) \cdot \mathbf{A}_k^h \\
&\quad \left[\frac{\partial \mathbf{U}^h}{\partial t} + \mathbf{A}_i^h \frac{\partial \mathbf{U}^h}{\partial x_i} - \frac{\partial}{\partial x_i} \left(\mathbf{K}_{ij}^h \frac{\partial \mathbf{U}^h}{\partial x_j} \right) - \mathbf{R}^h \right] \mathrm{d}Q \\
&+ \sum_{e=1}^{(n_{\mathrm{el}})_n} \int_{Q_n^e} \nu_{\mathrm{SHOC}} \left(\frac{\partial \mathbf{W}^h}{\partial x_i} \right) \cdot \left(\frac{\partial \mathbf{U}^h}{\partial x_i} \right) \mathrm{d}Q = 0 \,. \qquad (8)
\end{aligned}
$$

Here P_n is the lateral boundary of the space–time slab. The solution to Eq. (8) is obtained sequentially for all space–time slabs Q_0, Q_1, Q_2, ..., Q_{N-1}, and the computations start with $(\mathbf{U}^h)_0^- = \mathbf{U}_0^h$, where $\mathbf{U}_0$ is the specified initial value of the vector $\mathbf{U}$.

4 Stabilization parameters and shock-capturing

Various options for calculating the stabilization parameters and defining the shock-capturing terms in the context of the $(\mathrm{SUPG})_{82}$ formulation were introduced in [14, 15]. In this section we describe those options. For this purpose, we first define the acoustic speed as c, and define the unit vector $\mathbf{j}$ as

$$
\mathbf{j} = \frac{\nabla \rho^h}{\| \nabla \rho^h \|} \,. \qquad (9)
$$

As the first option in computing τ_{SUGN1} for each component of the test vector-function $\mathbf{W}$, the stabilization parameters $\tau^{\rho}{}_{\mathrm{SUGN1}}$, $\tau^{u}{}_{\mathrm{SUGN1}}$ and $\tau^{e}{}_{\mathrm{SUGN1}}$ (associated with ρ, $\rho\mathbf{u}$ and ρe, respectively) are defined by the following expression:

$$
\tau^{\rho}{}_{\mathrm{SUGN1}} = \tau^{u}{}_{\mathrm{SUGN1}} = \tau^{e}{}_{\mathrm{SUGN1}} = \left(\sum_{a=1}^{n_{\mathrm{en}}} |\mathbf{u}^h \cdot \nabla N_a| \right)^{-1} \,. \qquad (10)
$$

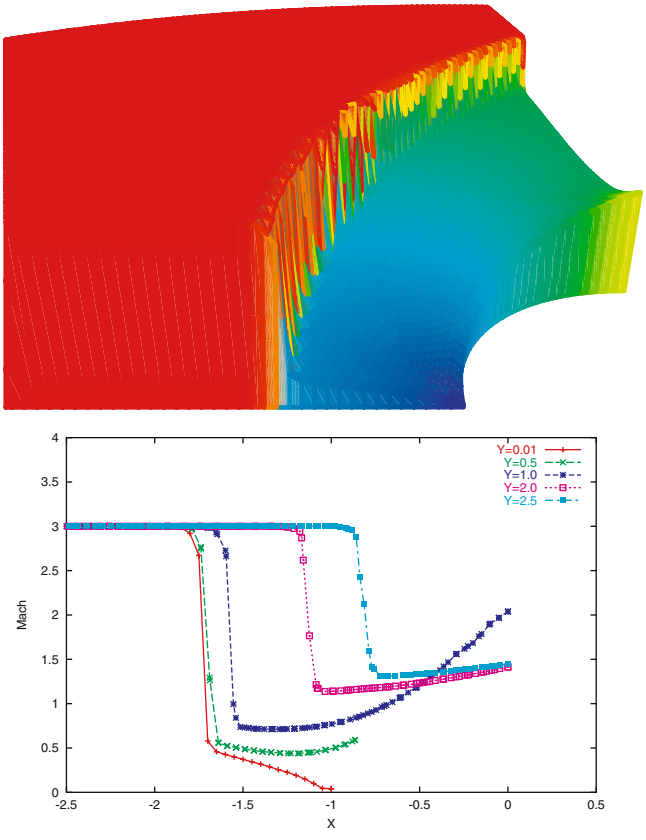

Fig. 10 Two-dimensional flow around a cylinder at $M = 3$. Mach elevation and line plots. Computed with the unstructured mesh and $YZ\beta$ Shock-Capturing with $b_{\mathrm{M}} = 1$, $b_{\mathrm{R}} = 1$, $\rho_{\mathrm{sca}} = \rho_2$

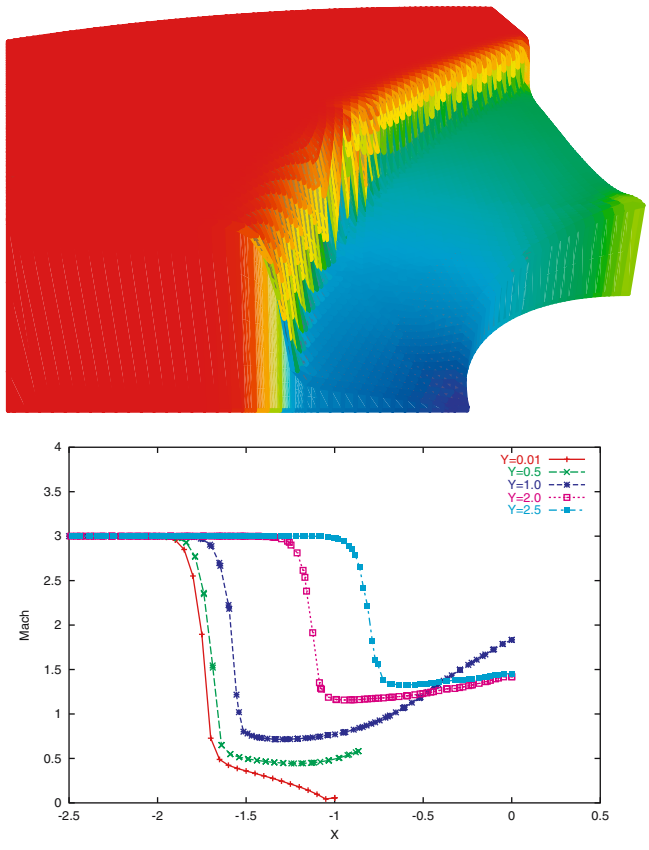

Fig. 11 Two-dimensional flow around a cylinder at $M = 3$. Mach elevation and line plots. Computed with the unstructured mesh and $\tau_{82\text{-MOD}}$ and δ_{91}

As the second option, they are defined as

$$\tau^{\rho}{}_{\mathrm{SUGN1}} = \tau^{u}{}_{\mathrm{SUGN1}} = \tau^{e}{}_{\mathrm{SUGN1}} = \left(\sum_{a=1}^{n_{\mathrm{en}}} \left(c\,|\mathbf{j} \cdot \nabla N_a| + |\mathbf{u}^h \cdot \nabla N_a| \right) \right)^{-1} . \tag{11}$$

In computing τ_{SUGN2}, the parameters $\tau^{\rho}{}_{\mathrm{SUGN2}}$, $\tau^{u}{}_{\mathrm{SUGN2}}$ and $\tau^{e}{}_{\mathrm{SUGN2}}$ are defined as follows:

$$\tau^{\rho}{}_{\mathrm{SUGN2}} = \tau^{u}{}_{\mathrm{SUGN2}} = \tau^{e}{}_{\mathrm{SUGN2}} = \frac{\Delta t}{2} , \tag{12}$$

where Δt is the time step. In computing τ_{SUGN3}, the parameter $\tau^{u}{}_{\mathrm{SUGN3}}$ is defined by using the expression

$$\tau^{u}{}_{\mathrm{SUGN3}} = \frac{h^2_{\mathrm{RGN}}}{4\nu} , \tag{13}$$

where

$$h_{\mathrm{RGN}} = 2 \left(\sum_{a=1}^{n_{\mathrm{en}}} |\mathbf{r} \cdot \nabla N_a| \right)^{-1} , \quad \mathbf{r} = \frac{\nabla \| \mathbf{u}^h \|}{\| \nabla \| \mathbf{u}^h \| \|} . \tag{14}$$

The parameter $\tau^{e}{}_{\mathrm{SUGN3}}$ is defined as

$$\tau^{e}{}_{\mathrm{SUGN3}} = \frac{(h^{e}{}_{\mathrm{RGN}})^2}{4\nu^e} , \tag{15}$$

where ν^e is the "kinematic viscosity" for the energy equation,

$$h^{e}{}_{\mathrm{RGN}} = 2 \left(\sum_{a=1}^{n_{\mathrm{en}}} |\mathbf{r}^e \cdot \nabla N_a| \right)^{-1} , \quad \mathbf{r}^e = \frac{\nabla \theta^h}{\| \nabla \theta^h \|} , \tag{16}$$

and θ is the temperature.The parameters $(\tau^{\rho}_{\mathrm{SUPG}})_{\mathrm{UGN}}$, $(\tau^{u}_{\mathrm{SUPG}})_{\mathrm{UGN}}$ and $(\tau^{e}_{\mathrm{SUPG}})_{\mathrm{UGN}}$ are calculated from their components by using the "*r-switch*":

$$(\tau^{\rho}_{\mathrm{SUPG}})_{\mathrm{UGN}} = \left(\frac{1}{(\tau^{\rho}{}_{\mathrm{SUGN1}})^r} + \frac{1}{(\tau^{\rho}{}_{\mathrm{SUGN2}})^r} \right)^{-\frac{1}{r}} , \tag{17}$$

$$(\tau^{u}_{\mathrm{SUPG}})_{\mathrm{UGN}} = \left(\frac{1}{(\tau^{u}{}_{\mathrm{SUGN1}})^r} + \frac{1}{(\tau^{u}{}_{\mathrm{SUGN2}})^r} + \frac{1}{(\tau^{u}{}_{\mathrm{SUGN3}})^r} \right)^{-\frac{1}{r}} , \tag{18}$$

$$(\tau^{e}_{\mathrm{SUPG}})_{\mathrm{UGN}} = \left(\frac{1}{(\tau^{e}{}_{\mathrm{SUGN1}})^r} + \frac{1}{(\tau^{e}{}_{\mathrm{SUGN2}})^r} + \frac{1}{(\tau^{e}{}_{\mathrm{SUGN3}})^r} \right)^{-\frac{1}{r}} . \tag{19}$$

Typically, $r = 2$.

In defining the shock-capturing term, first the "shock-capturing viscosity" ν_{SHOC} is defined:

$$\nu_{\mathrm{SHOC}} = \left\| \mathbf{Y}^{-1}\mathbf{Z} \right\| \left(\sum_{i=1}^{n_{sd}} \left\| \mathbf{Y}^{-1} \frac{\partial \mathbf{U}^h}{\partial x_i} \right\|^2 \right)^{(\beta/2)-1} \left(\frac{h_{\mathrm{SHOC}}}{2} \right)^{\beta} , \tag{20}$$

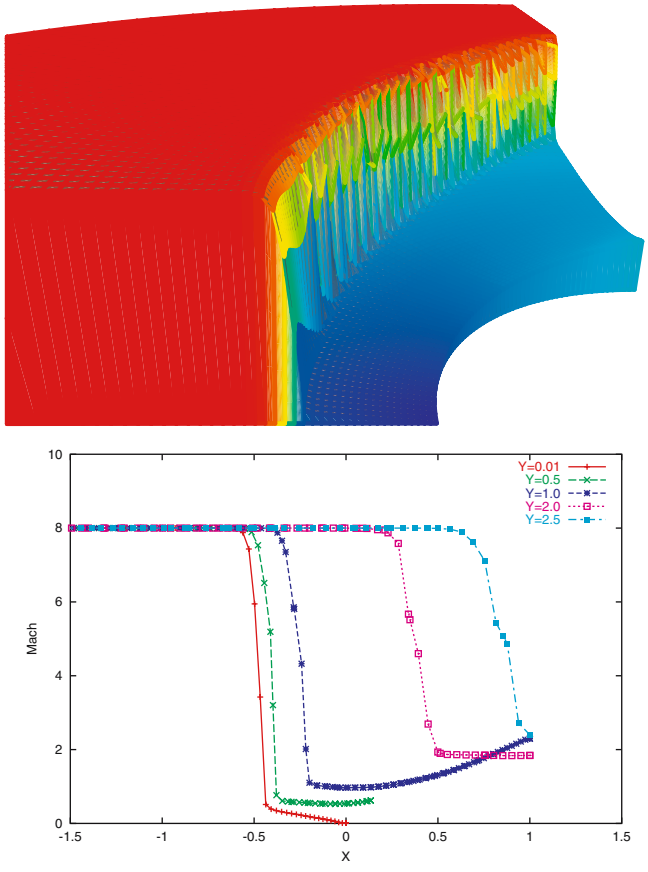

Fig. 12 Two-dimensional flow around a cylinder at $M = 8$. Mach elevation and line plots. Computed with the structured mesh and $YZ\beta$ Shock-Capturing with $b_{\text{M}} = 2$, $b_{\text{R}} = 0$

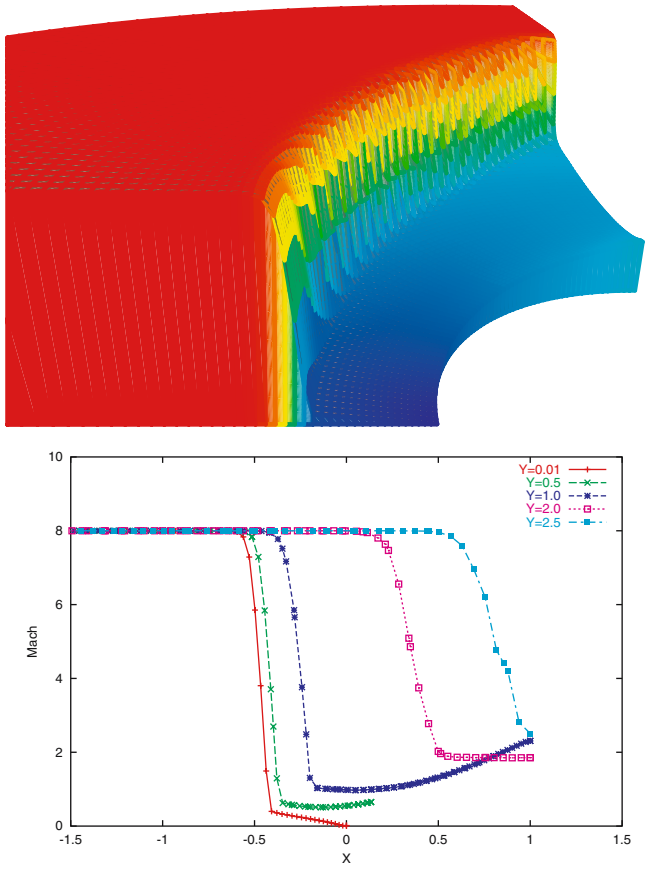

Fig. 13 Two-dimensional flow around a cylinder at $M = 8$. Mach elevation and line plots. Computed with the structured mesh and $YZ\beta$ Shock-Capturing with $b_{\text{M}} = 1$, $b_{\text{R}} = 0$

where $\mathbf{Y}$ is a diagonal scaling matrix constructed from the reference values of the components of $\mathbf{U}$:

$$\mathbf{Y} = \begin{bmatrix} (U_1)_{\text{ref}} & 0 & 0 & 0 & 0 \\ 0 & (U_2)_{\text{ref}} & 0 & 0 & 0 \\ 0 & 0 & (U_3)_{\text{ref}} & 0 & 0 \\ 0 & 0 & 0 & (U_4)_{\text{ref}} & 0 \\ 0 & 0 & 0 & 0 & (U_5)_{\text{ref}} \end{bmatrix}, \tag{21}$$

$$\mathbf{Z} = \frac{\partial \mathbf{U}^h}{\partial t} + \mathbf{A}_i^h \frac{\partial \mathbf{U}^h}{\partial x_i} \tag{22}$$

or

$$\mathbf{Z} = \mathbf{A}_i^h \frac{\partial \mathbf{U}^h}{\partial x_i} \tag{23}$$

and

$$h_{\text{SHOC}} = h_{\text{JGN}}\,, \tag{24}$$

$$h_{\text{JGN}} = 2\left(\sum_{a=1}^{n_{\text{en}}} |\mathbf{j}\cdot\nabla N_a|\right)^{-1}. \tag{25}$$

The parameter β is set as $\beta = 1$ for smoother shocks and $\beta = 2$ for sharper shocks. In a variation of the expression given by Eq. (20), ν_{SHOC} is defined by the following expression:

$$\nu_{\text{SHOC}} = \left\|\mathbf{Y}^{-1}\mathbf{Z}\right\|\left(\sum_{i=1}^{n_{\text{sd}}}\left\|\mathbf{Y}^{-1}\frac{\partial \mathbf{U}^h}{\partial x_i}\right\|^2\right)^{(\beta/2)-1}\left\|\mathbf{Y}^{-1}\mathbf{U}^h\right\|^{1-\beta} \times\left(\frac{h_{\text{SHOC}}}{2}\right)^{\beta}. \tag{26}$$

The compromise between the $\beta = 1$ and $\beta = 2$ selections is defined as the following averaged expression for ν_{SHOC} :

$$\nu_{\text{SHOC}} = \frac{1}{2}\left((\nu_{\text{SHOC}})_{\beta=1} + (\nu_{\text{SHOC}})_{\beta=2}\right). \tag{27}$$

We also propose versions of ν_{SHOC} that take into account the Mach number and shock intensity across a shock. In doing that, we modify ν_{SHOC} given by Eqs. (20) and (26) as follows:

$$\nu_{\text{SHOC}} \leftarrow \nu_{\text{SHOC}} \left(1+\left(\frac{\|\nabla\rho^h\|\, h_{\text{SHOC}}}{\rho_{\text{ref}}}\right)\langle M^{1/b_{\text{M}}} - 1\rangle\right)^{2/b_{\text{F}}}, \tag{28}$$

where M is the Mach number and "$\langle\cdots\rangle$" is the Macaulay bracket:

$$\langle x - y\rangle = \begin{cases} 0, & x \le y \\ x - y, & x > y \end{cases} \tag{29}$$

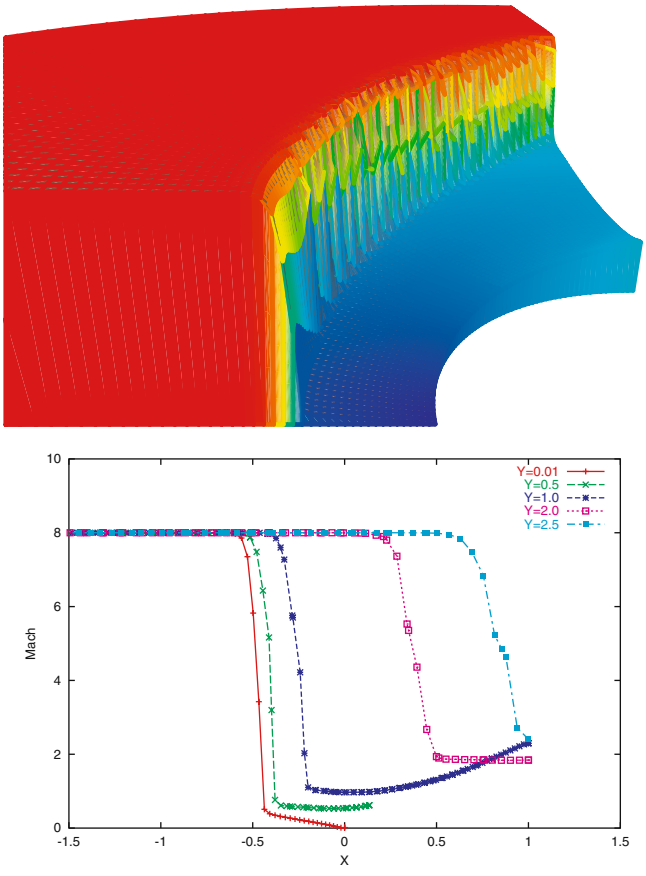

Fig. 14 Two-dimensional flow around a cylinder at $M = 8$. Mach elevation and line plots. Computed with the structured mesh and $YZ\beta$ Shock-Capturing with $b_{\text{M}} = 1$, $b_{\text{R}} = 1$, $\rho_{\text{sca}} = \rho_2$

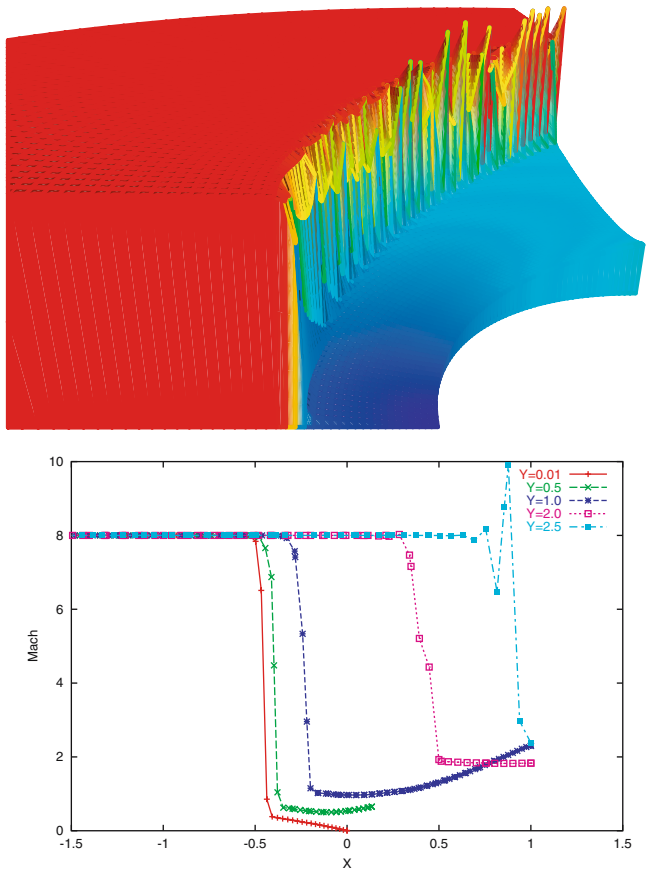

Fig. 15 Two-dimensional flow around a cylinder at $M = 8$. Mach elevation and line plots. Computed with the structured mesh and $\tau_{82\text{-MOD}}$ and δ_{91}

The reference density ρ_{ref} is defined as

$$\rho_{\text{ref}} = \rho_{\text{inf}} \left(\frac{\rho_{\text{sca}}}{\rho_{\text{inf}}} \right)^{b_{\text{R}}/2} , \tag{30}$$

where ρ_{inf} is the density at the inflow and ρ_{sca} is a scaling density. In defining ρ_{sca}, one of the options we consider is $\rho_{\text{sca}} = \rho_{\text{inf}}$. For flows with shocks, we also consider the options $\rho_{\text{sca}} = \rho_2$ and $\rho_{\text{sca}} = \rho_2 - \rho_1$, where ρ_1 and ρ_2 are the density values before and after a normal shock corresponding to the inflow Mach number. The parameters b_{M}, b_{F} and b_{R} can each be set to 1 for smoother shocks and 2 for sharper shocks. Equation (28), without the exponent $2/b_{\text{F}}$, was originally introduced in [17]. With this expression, the definition of the shock-capturing viscosity takes into account the Mach number and shock intensity across a shock. The shock intensity is represented by the term $\left(\frac{\| \nabla \rho^h \| \, h_{\text{SHOC}}}{\rho_{\text{ref}}} \right)$, which is a scaled measure of the jump in density. The Mach number is represented by the term $\langle M^{1/b_{\text{M}}} - 1 \rangle$, which becomes active for $M > 1$. Based on Eq. (20), a separate ν_{SHOC} can be calculated for each component of the test vector-function $\mathbf{W}$:

$$(\nu_{\text{SHOC}})_I = \left| \left(\mathbf{Y}^{-1}\mathbf{Z} \right)_I \right| \left(\sum_{i=1}^{n_{\text{sd}}} \left| \left(\mathbf{Y}^{-1} \frac{\partial \mathbf{U}^h}{\partial x_i} \right)_I \right|^2 \right)^{(\beta/2)-1} \left(\frac{h_{\text{SHOC}}}{2} \right)^{\beta} , \quad I = 1, 2, \ldots n_{\text{sd}} + 2 . \tag{31}$$

Similarly, a separate ν_{SHOC} for each component of $\mathbf{W}$ can be calculated based on Eq. (26):

$$(\nu_{\text{SHOC}})_I = \left| \left(\mathbf{Y}^{-1}\mathbf{Z} \right)_I \right| \left(\sum_{i=1}^{n_{\text{sd}}} \left| \left(\mathbf{Y}^{-1} \frac{\partial \mathbf{U}^h}{\partial x_i} \right)_I \right|^2 \right)^{(\beta/2-1)} \times \left| \left(\mathbf{Y}^{-1}\mathbf{U}^h \right)_I \right|^{1-\beta} \left(\frac{h_{\text{SHOC}}}{2} \right)^{\beta} , \quad I = 1, 2, \ldots n_{\text{sd}} + 2 . \tag{32}$$

Given ν_{SHOC}, the shock-capturing term is defined as

$$S_{\text{SHOC}} = \sum_{e=1}^{n_{\text{el}}} \int_{\Omega^e} \nabla \mathbf{W}^h : \left(\boldsymbol{\kappa}_{\text{SHOC}} \cdot \nabla \mathbf{U}^h \right) \mathrm{d}\Omega , \tag{33}$$

where $\boldsymbol{\kappa}_{\text{SHOC}}$ is defined as $\boldsymbol{\kappa}_{\text{SHOC}} = \nu_{\text{SHOC}} \, \mathbf{I}$. As a possible alternative, it is defined as $\boldsymbol{\kappa}_{\text{SHOC}} = \nu_{\text{SHOC}} \, \mathbf{jj}$. If the option given by Eq. (31) or Eq. (32) is exercised, then ν_{SHOC} becomes an

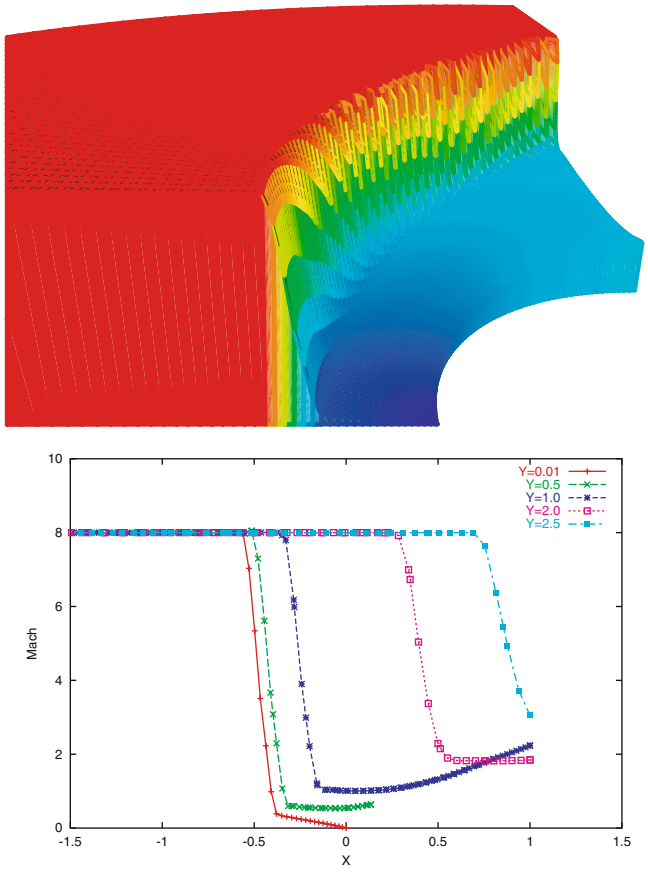

Fig. 16 Two-dimensional flow around a cylinder at $M = 8$. Mach elevation and line plots. Computed with the structured mesh and OVERFLOW

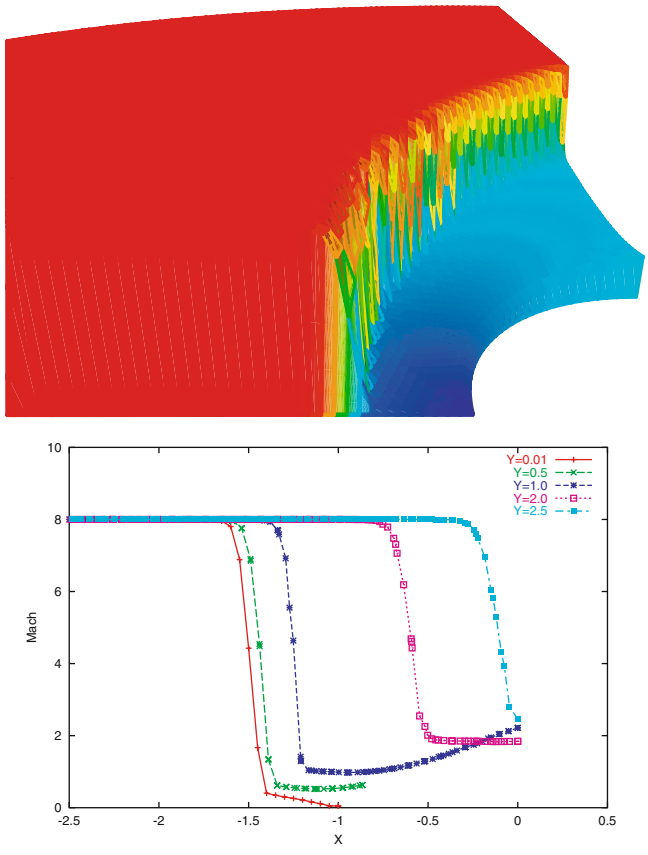

Fig. 17 Two-dimensional flow around a cylinder at $M = 8$. Mach elevation and line plots. Computed with the unstructured mesh and $YZ\beta$ Shock-Capturing with $b_{\text{M}} = 2$, $b_{\text{R}} = 0$

$(n_{\text{sd}} + 2) \times (n_{\text{sd}} + 2)$ diagonal matrix, and the matrix $\boldsymbol{\kappa}_{\text{SHOC}}$ becomes augmented from an $n_{\text{sd}} \times n_{\text{sd}}$ matrix to an $(n_{\text{sd}} \times (n_{\text{sd}} + 2)) \times ((n_{\text{sd}} + 2) \times n_{\text{sd}})$ matrix.

To preclude compounding, ν_{SHOC} can be modified as follows:

$$\nu_{\text{SHOC}} \leftarrow \nu_{\text{SHOC}} - \text{switch}\left(\tau_{\text{SUPG}}\,(\mathbf{j}\cdot\mathbf{u})^2,\, \tau_{\text{SUPG}}(|\mathbf{j}\cdot\mathbf{u}|-c)^2,\, \nu_{\text{SHOC}}\right), \tag{34}$$

where the "*switch*" function is defined as the "*min*" function or as the "*r-switch*" used earlier in this section. For viscous flows, the above modification would be made separately with each of $\tau^{\rho}_{\text{SUPG}}$, τ^{u}_{SUPG} and τ^{e}_{SUPG}, and this would result in ν_{SHOC} becoming a diagonal matrix even if the option given by Eq. (31) or (32) is not exercised.

5 Test computations

The test computations were carried out by using the space–time SUPG formulation described in Sect. 3. In all computations, as stabilization parameters, we use Eq. (11), and in Eqs. (17)–(19) we do not include τ_{SUGN2}. Also in all computations, we use Eq. (20) with $\beta = 1$, which is equivalent to using Eq. (26) with $\beta = 1$, use for $\mathbf{Z}$ the expression given by Eq. (23), and set $\boldsymbol{\kappa}_{\text{SHOC}} = \nu_{\text{SHOC}}\,\mathbf{I}$. In Eq. (21), we set $(U_1)_{\text{ref}}$ to the inflow value of ρ, set $(U_2)_{\text{ref}}$, $(U_3)_{\text{ref}}$ and $(U_4)_{\text{ref}}$ to the inflow value of ρu_1, and set $(U_5)_{\text{ref}}$ to the inflow value of ρe. In Eq. (28), unless stated otherwise, we set $b_{\text{F}} = 2$.

The results are compared to those obtained with the $\tau_{\text{82-MOD}}$ and δ_{91} combination. The version of $\tau_{\text{82-MOD}}$ used in this paper for comparison is similar to the one given in [22]:

$$\tau_{\text{82-MOD}} = \max\,(0,\, \tau_a - \tau_\delta)\ , \tag{35}$$

where

$$\tau_a = \frac{h_{\text{BGN}}}{2u_{\text{cc}}}, \quad \tau_\delta = \frac{\delta_{91}}{(u_{\text{cc}})^2},$$
$$u_{\text{cc}} = c + \left|\mathbf{u}^h \cdot \frac{\boldsymbol{\nabla}\|\mathbf{U}^h\|}{\|\,\boldsymbol{\nabla}\|\mathbf{U}^h\|\,\|}\right|, \tag{36}$$

$$h_{\text{BGN}} = 2\left(\sum_{a=1}^{n_{\text{en}}}\left|\frac{\boldsymbol{\nabla}\|\mathbf{U}^h\|}{\|\,\boldsymbol{\nabla}\|\mathbf{U}^h\|\,\|}\cdot\boldsymbol{\nabla}N_a\right|\right)^{-1}. \tag{37}$$

For completeness, we also provide here the expression for δ_{91} [7]:

$$\delta_{91} = \left\|\mathbf{A}^h_k\,\frac{\partial\mathbf{U}^h}{\partial x_k}\right\|_{\widetilde{\mathbf{A}}_0^{-1}} \Big/ \left(\sum_{j=1}^{n_{\text{sd}}}\left\|\frac{\partial\xi_j}{\partial x_k}\,\frac{\partial\mathbf{U}^h}{\partial x_k}\right\|^2_{\widetilde{\mathbf{A}}_0^{-1}}\right)^{\frac{1}{2}}, \tag{38}$$

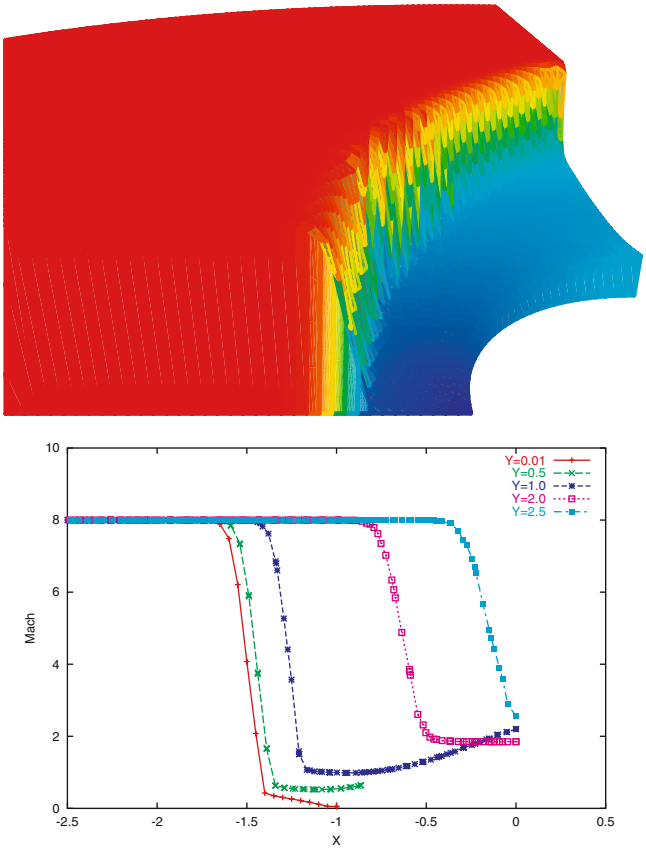

Fig. 18 Two-dimensional flow around a cylinder at $M = 8$. Mach elevation and line plots. Computed with the unstructured mesh and $YZ\beta$ Shock-Capturing with $b_{\mathrm{M}} = 1$, $b_{\mathrm{R}} = 0$

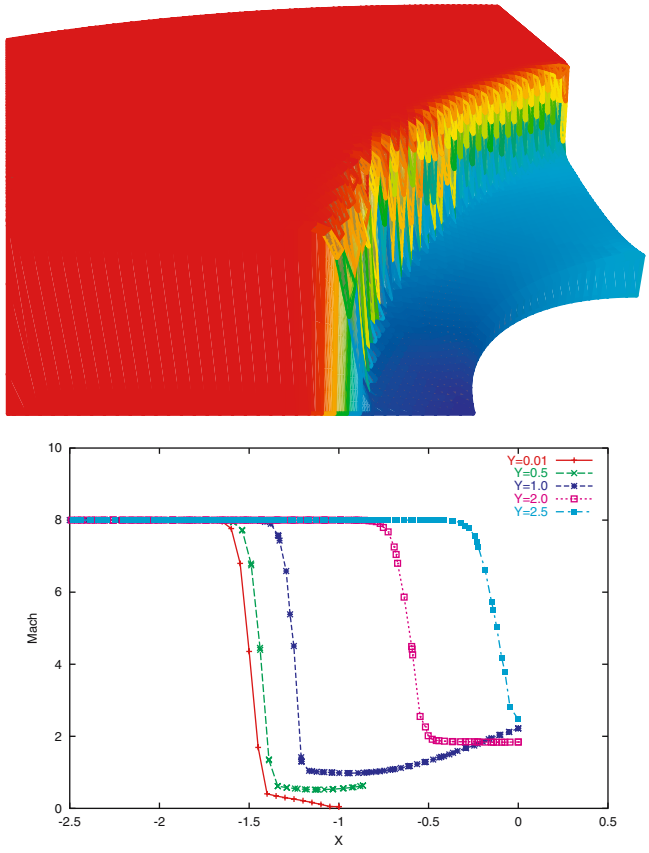

Fig. 19 Two-dimensional flow around a cylinder at $M = 8$. Mach elevation and line plots. Computed with the unstructured mesh and $YZ\beta$ Shock-Capturing with $b_{\mathrm{M}} = 1$, $b_{\mathrm{R}} = 1$, $\rho_{\mathrm{sca}} = \rho_2$

where ξ_j values are the element coordinates, and $\widetilde{\mathbf{A}}_0$ is the Jacobian of the transformation from the entropy variables to the conservation variables.

The results are also compared to those obtained with the OVERFLOW code [18]. The OVERFLOW cases were run with central differencing and matrix dissipation, which mimics the Roe–upwinding scheme but is computationally more economical and generally more robust. The matrix dissipation minimum limit on the linear and nonlinear eigenvalues were each set to 0.3, and the spectral radius term was set to 0.0. All other parameters were left at their defaults values. Table 1 lists the parameters that were changed from their default values.

As test problems, we consider steady-state cases. The solutions are obtained with time-marching to the steady-state. At each time step, the coupled nonlinear equations involved are solved with the Newton–Raphson method. An iterative technique with nodal-block-diagonal preconditioner and GMRES update method [23] is employed for solving the linear equation system involved at each Newton–Raphson iteration.

5.1 Two-dimensional flow around a cylinder

We compute this case at $M = 3$ and $M = 8$, with structured and unstructured meshes. Figures 1 and 2 show those meshes. The structured mesh has 4,096 quadrilateral elements and 4,225 nodes, while the unstructured mesh has 17,520 triangular elements and 8,935 nodes. In computational units, the inflow density and velocity are 1.0 and (M, 0). The inflow value of the total energy is 6.286 at $M = 3$ and 33.786 at $M = 8$. At the inflow boundary, we specify all conservation variables to be equal to their inflow values. On the cylinder surface and horizontal boundary, we specify the normal component of the velocity to be zero. No boundary conditions are specified at the outflow boundary. The number of Newton–Raphson iterations and the outer and inner GMRES iterations are 3, 1, and 5, respectively.

Figures 3–7 show the results obtained for $M = 3$ with the structured mesh. The results shown in Figures 3, 4, 5 were obtained with $YZ\beta$ Shock-Capturing. Figure 6 shows the results obtained with $\tau_{82\text{-MOD}}$ and δ_{91}. Figure 7 shows the results obtained with OVERFLOW. The $YZ\beta$ results obtained with $b_{\mathrm{M}} = 2$, $b_{\mathrm{R}} = 0$ are very close to those obtained with $b_{\mathrm{M}} = 1$, $b_{\mathrm{R}} = 1$, $\rho_{\mathrm{sca}} = \rho_2$. They are also very close to the OVERFLOW results, but have slightly crisper shocks. Furthermore, they are also very close to the results obtained with $\tau_{82\text{-MOD}}$ and δ_{91}, but again have very slightly crisper shocks. The $YZ\beta$ results obtained with $b_{\mathrm{M}} = 1$, $b_{\mathrm{R}} = 0$ show slightly more dissipation than the other two $YZ\beta$ results and are closer to the OVERFLOW results.

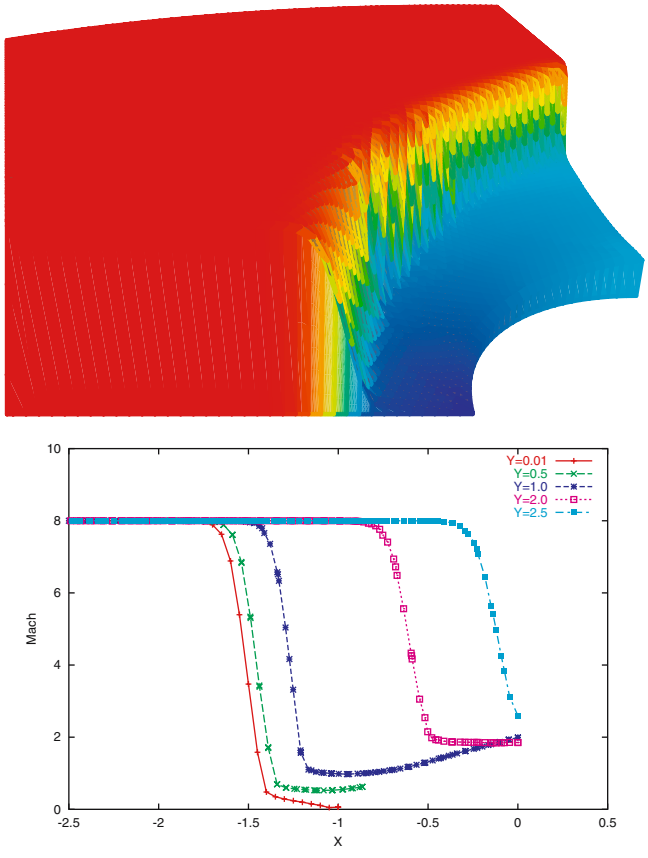

Fig. 20 Two-dimensional flow around a cylinder at $M = 8$. Mach elevation and line plots. Computed with the unstructured mesh and $\tau_{82\text{-MOD}}$ and δ_{91}

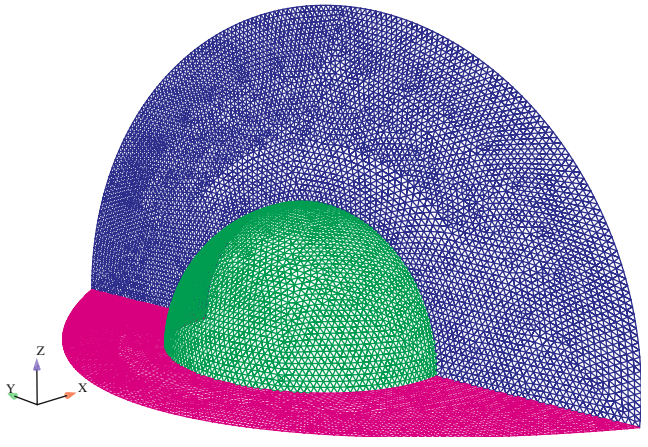

Fig. 21 Three-dimensional flow around a sphere. Unstructured mesh with 461,913 tetrahedral elements and 86,176 nodes

Figures 8–11 show the results obtained for $M = 3$ with the unstructured mesh. The results shown in Figs. 8–10 were obtained with the same three types of $YZ\beta$ Shock-Capturing we had for the structured mesh. Figure 11 shows the results obtained with $\tau_{82\text{-MOD}}$ and δ_{91}. All three $YZ\beta$ results are very close. They are also very close to the OVERFLOW

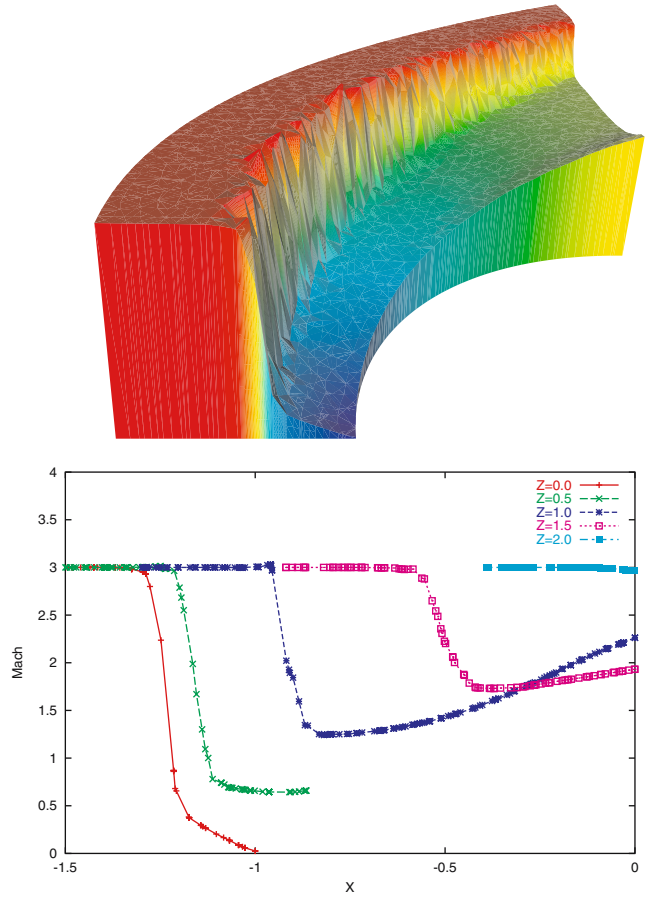

Fig. 22 Three-dimensional flow around a sphere at $M = 3$. Mach elevation on $y = 0$ plane and line plots. Computed with $YZ\beta$ Shock-Capturing with $b_M = 1$, $b_R = 0$

results obtained with the structured mesh. The results obtained with $\tau_{82\text{-MOD}}$ and δ_{91} exhibit significant dissipation. This is consistent with the observations we had in [17] regarding the performance of this method with unstructured meshes.

Figures 12–16 show the results obtained for $M = 8$ with the structured mesh. The results shown in Figs. 12–14 were obtained with the same three types of $YZ\beta$ Shock-Capturing we had for $M = 8$. Figure 15 shows the results obtained with $\tau_{82\text{-MOD}}$ and δ_{91}. Figure 16 shows the results obtained with OVERFLOW. All three $YZ\beta$ results are very close. They are also very close to the OVERFLOW results. The results obtained with $\tau_{82\text{-MOD}}$ and δ_{91} exhibit significant overshoots near the shock.

Figures 17–20 show the results obtained for $M = 8$ with the unstructured mesh. The results shown in Figs. 17–19 were obtained with the same three types of $YZ\beta$ Shock-Capturing we had for the structured mesh. Figure 20 shows the results obtained with $\tau_{82\text{-MOD}}$ and δ_{91}. All three $YZ\beta$ results are very close. They are also very close to the OVERFLOW results obtained with the structured mesh. The results obtained with $\tau_{82\text{-MOD}}$ and δ_{91} exhibit significant dissipation. This is consistent with the observations we had for $M = 3$ case.

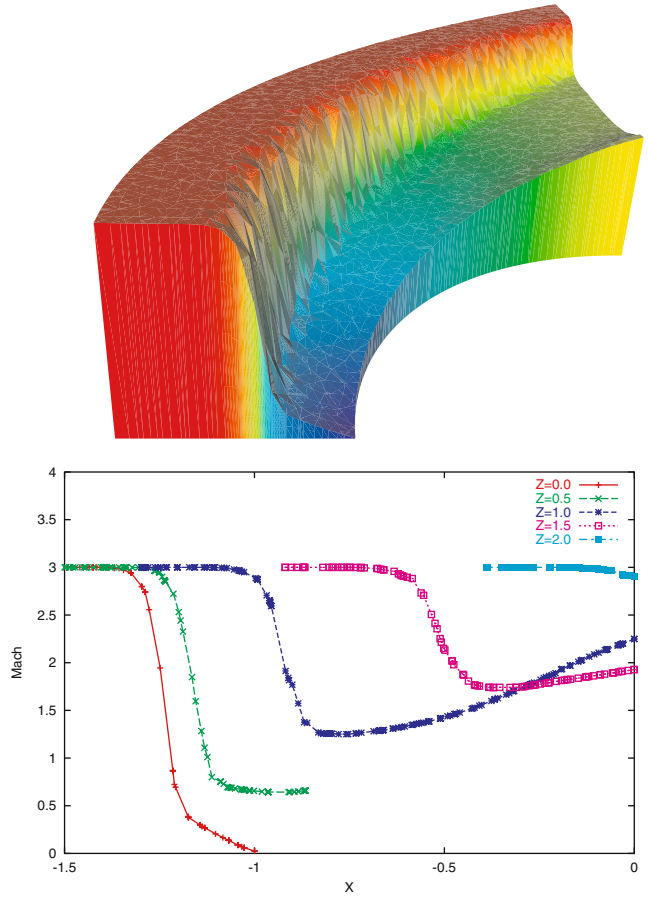

Fig. 23 Three-dimensional flow around a sphere at $M = 3$. Mach elevation on $y = 0$ plane and line plots. Computed with $YZ\beta$ Shock-Capturing with $b_{\text{M}} = 1$, $b_{\text{R}} = 0$ and $b_{\text{F}} = 1$

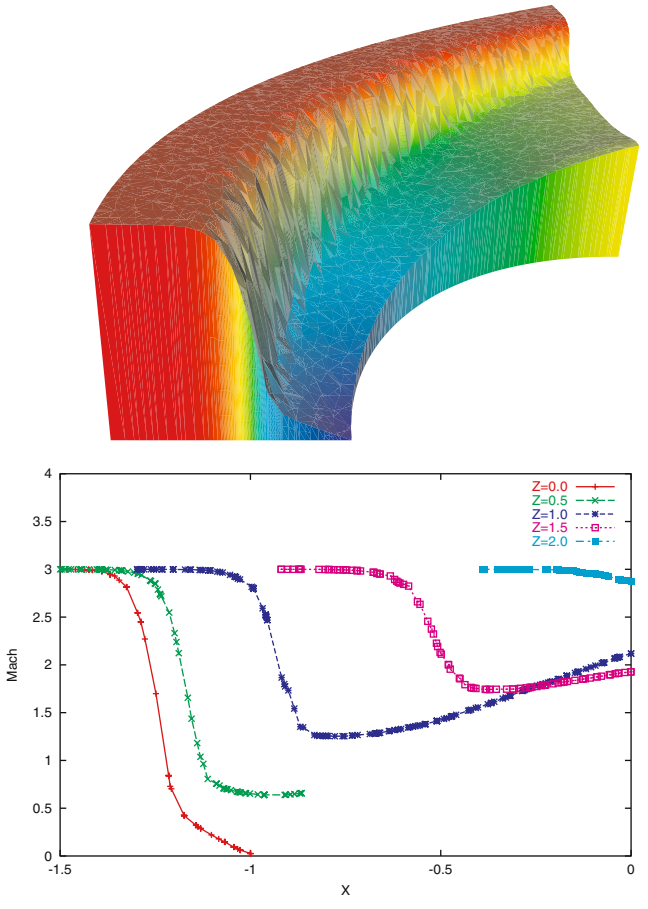

Fig. 24 Three-dimensional flow around a sphere at $M = 3$. Mach elevation on $y = 0$ plane and line plots. Computed with $\tau_{\text{82-MOD}}$ and δ_{91}

5.2 Three-dimensional flow around a sphere

We compute this case at $M = 3$, with an unstructured mesh. Figure 21 shows the mesh, which has 461,913 tetrahedral elements and 86,176 nodes.In computational units, the inflow density and velocity are 1.0 and (3, 0, 0). The inflow value of the total energy is 6.286. At the inflow boundary, we specify all conservation variables to be equal to their inflow values. On the sphere surface and horizontal boundary, we specify the normal component of the velocity to be zero. No boundary conditions are specified at the outflow boundary. The number of Newton–Raphson iterations and the outer and inner GMRES iterations are 3, 1, and 10, respectively.

Figure 22 shows the results obtained with the second one of the three types $YZ\beta$ Shock-Capturing we tested in the 2D cases. The $YZ\beta$ parameters are set as $b_{\text{M}} = 1$ and $b_{\text{R}} = 0$. We have some mild overshoots near the shock. We think this is because the mesh is too coarse. In the 3D test cases, to have a mesh resolution comparable to the mesh resolution we had for the unstructured mesh used in the 2D test cases, we would need roughly 10 times more nodes than we have now. To decrease the overshoots, we activate the parameter b_{F} by setting it as $b_{\text{F}} = 1$. Figure 23 shows the results obtained with $YZ\beta$ Shock-Capturing with $b_{\text{M}} = 1$, $b_{\text{R}} = 0$, and $b_{\text{F}} = 1$. Figure 24 shows the results obtained with $\tau_{\text{82-MOD}}$ and δ_{91}. These results exhibit significant dissipation compared to the two $YZ\beta$ results, especially compared to the first one.

6 Concluding remarks

We carried out a comprehensive set of numerical experiments with inviscid supersonic flows around cylinders and spheres to evaluate the performance of $YZ\beta$ Shock-Capturing, which was introduced recently for the SUPG formulation of compressible flows based on conservation variables. As test cases, we computed 2D flow around a cylinder at Mach number 3 and 8, using a structured mesh with quadrilateral elements and an unstructured mesh with triangular elements. Also as test cases, we computed 3D flow around a sphere at Mach number 3, using an unstructured mesh with tetrahedral elements. Our comprehensive set of computations included testing a version of $YZ\beta$ Shock-Capturing that takes into account the Mach number and shock intensity across a shock. In all test cases, we compared our results to those obtained

with τ_{82} and δ_{91}. In addition to being much simpler, $YZ\beta$ Shock-Capturing yields better shock quality, and even more substantial improvements for unstructured meshes with triangular and tetrahedral elements. In 2D cases, we compared the $YZ\beta$ Shock-Capturing results also to those obtained with the OVERFLOW code. These comparisons show that the quality of the shocks obtained with $YZ\beta$ Shock-Capturing are very close to what one obtains with the OVERFLOW code.

Acknowledgements This work was supported by the US Army Natick Soldier Center (Contract No. DAAD16-03-C-0051) and NASA Johnson Space Center (Grant No. NAG9-1435).

References

1. Hughes TJR, Brooks AN (1979) A Multi-dimensional Upwind Scheme with no Crosswind Diffusion. In: Hughes TJR (ed) Finite element methods for convection dominated flows, AMD-vol 34. ASME, New York, pp 19–35
2. Brooks AN, Hughes TJR (1982) Streamline Upwind/Petrov–Galerkin Formulations for convection dominated flows with Particular emphasis on the incompressible Navier–Stokes Equations. Comput Methods Appl Mech Eng 32:199–259
3. Tezduyar TE, Hughes TJR (1982) Development of time-accurate finite element techniques for first-order hyperbolic systems with particular emphasis on the compressible Euler equations. NASA Technical Report NASA-CR-204772, NASA, Also available online: http://ntrs.nasa.gov/archive/nasa/casi.ntrs.nasa.gov/19970023187_1997034954.pdf
4. Tezduyar TE, Hughes TJR (1983) Finite element formulations for convection dominated flows with particular emphasis on the compressible Euler equations. In: Proceedings of AIAA 21st aerospace sciences meeting, AIAA Paper 83-0125, Reno, Nevada
5. Hughes TJR, Tezduyar TE (1984) Finite element methods for first-order hyperbolic systems with particular emphasis on the compressible Euler equations. Comput Methods Appl Mech Eng 45:217–284
6. Hughes TJR, Franca LP, Mallet M (1987) A New Finite element formulation for computational fluid dynamics: VI. Convergence analysis of the generalized SUPG formulation for linear time-dependent multi-dimensional advective-diffusive systems. Comput Methods Appl Mech Eng 63:97–112
7. Le Beau GJ, Tezduyar TE (1991) Finite element computation of compressible flows with the SUPG formulation. In: Advances in finite element analysis in fluid dynamics, FED-vol.123. ASME, New York, pp 21–27
8. Le Beau GJ, Ray SE, Aliabadi SK, Tezduyar TE (1993) SUPG finite element computation of compressible flows with the entropy and conservation variables formulations. Comput Methods Appl Mech Eng 104:397–422
9. Tezduyar TE, Park YJ (1986) Discontinuity capturing finite element formulations for nonlinear convection-diffusion-reaction equations. Comput Methods Appl Mech Eng 59:307–325
10. Hughes TJR, Mallet M (1986) A new finite element formulation for computational fluid dynamics: III. The generalized streamline operator for multidimensional advective–diffusive systems. Comput Methods Appl Mech Eng 58:305–328
11. Shakib F, Hughes TJR, Johan Z (1991) A new finite element formulation for computational fluid dynamics: X. The compressible euler and Navier–Stokes equations. Comput Methods Appl Mech Eng 89:141–219
12. Tezduyar TE (2001) Adaptive determination of the finite element stabilization parameters. In: Proceedings of the ECCOMAS computational fluid dynamics conference, Swansea, Wales.
13. Tezduyar TE (2003) Computation of moving boundaries and interfaces and stabilization parameters. Int J Numer Methods Fluids 43:555–575
14. Tezduyar TE (2004) Finite element methods for fluid dynamics with moving boundaries and interfaces. In: Stein E, De Borst R, Hughes TJR (eds) Encyclopedia of computational mechanics, volume 3: Fluids, Chapter 17. Wiley, New York
15. Tezduyar TE (2004) Determination of the stabilization and shock-capturing parameters in SUPG formulation of compressible flows. In: Proceedings of the European Congress on computational methods in applied sciences and engineering, ECCOMAS 2004, Jyvaskyla, Finland
16. Tezduyar TE, Senga M (2005) Stabilization and shock-capturing parameters in SUPG formulation of compressible flows. Comput Methods Appl Mech Eng ~~(in press)~~ **195** (2006) 1621-1632.
17. Tezduyar TE, Senga M (2005) SUPG finite element computation of inviscid supersonic flows with YZβ shock-capturing. Comput Fluids (in press)
18. Buning PG, Jespersen DC, Pulliam TH, Klopfer GH, Chan WM, Slotnick JP, Krist SE, Renze KJ (2000) OVERFLOW user's manual, Version 1.8s, NASA Langley Research Center, Hampton, Virginia
19. Tezduyar TE (1992) Stabilized finite element formulations for incompressible flow computations. Adv Appl Mech 28:1–44
20. Tezduyar TE, Behr M, Liou J (1992) A new strategy for finite element computations involving moving boundaries and interfaces – the deforming-spatial-domain/space–time procedure: I. The concept and the preliminary numerical tests. Comput Methods Appl Mech Eng 94:339–351
21. Tezduyar TE, Behr M, Mittal S, Liou J (1992) A new strategy for finite element computations involving moving boundaries and interfaces – the deforming-spatial-domain/space–time procedure: II. Computation of free-surface flows, two-liquid flows, and flows with drifting cylinders. Comput Methods Appl Mech Eng 94:353–371
22. Aliabadi SK, Tezduyar TE (1995) Parallel fluid dynamics computations in aerospace applications.Int J Numer Methods Fluids 21:783–805
23. Saad Y, Schultz M (1986) GMRES: A generalized minimal residual algorithm for solving nonsymmetric linear systems. SIAM J Sci Stat Comput 7:856–869